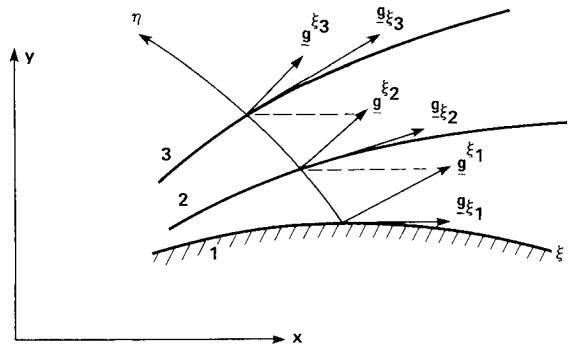

Fig. 3 Contravariant and covariant base vectors at three η locations.

$$V_1 \cdot g_{\xi 1} = (2V_2 - V_3) \cdot g_{\xi 1} \tag{3}$$

From the above discussion, one realizes that the removal of metric variation (by normalization) is needed only when a local metric is used. Note that, in a stretched rectangular grid, $g^{\xi 1}$, $g^{\xi 2}$, and $g^{\xi 3}$ are equal, and are parallel (and inverse in magnitude) to $g_{\xi 1}$. Therefore, the extrapolations used in Refs. 1 and 2 and in Eq. (3) will result in the same solution.

Next, we generalize the extrapolation and analyze the consequence of extrapolating such a velocity component, which may not be tangent to the body surface. As pointed out earlier, to be independent of the direction of mesh lines at locations 2 and 3, the only requirement is that we extrapolate velocity components in the same direction. Hence, one can substitute an arbitrary vector A for the covariant base vector $g_{\xi 1}$ in Eq. (3). Writing the decomposition procedure explicitly, the no-flux boundary condition [Eq. (1)] becomes

$$u_1 \eta_{x1} + v_1 \eta_{y1} = 0 \tag{4}$$

and the extrapolation of velocity components along a vector $A = (A_x e_i + A_y e_j)$ is

$$V_1 \cdot (A_x e_i + A_y e_j) = (2V_2 - V_3) \cdot (A_x e_i + A_y e_j)$$

or

$$A_x u_1 + A_y v_1 = A_x (2u_2 - u_3) + A_y (2v_2 - v_3) \tag{5}$$

Here e_i and e_j are the unit Cartesian base vectors. Equations (4) and (5) can be solved for u_1 and v_1, provided that A is not in the same direction as the surface normal $(\eta_{x1} e_i + \eta_{y1} e_j)$. Indeed, when A is the unit body normal, $A = (\eta_{x1} e_i + \eta_{y1} e_j)/\sqrt{\eta_{x1}^2 + \eta_{y1}^2}$, the right-hand side of Eq. (5) equals

$$R = \frac{\eta_{x1}(2u_2 - u_3) + \eta_{y1}(2v_2 - v_3)}{\sqrt{\eta_{x1}^2 + \eta_{y1}^2}}$$

and is a measure of error because of the inconsistency of the extrapolation of the normal velocity component. The employment of extrapolation as an extra numerical boundary condition indeed is based on the assumption that the error R, or strictly speaking $|R|/||(2V_2 - V_3)||$, is small. If $R = 0$, the tangential condition is automatically satisfied; therefore, one can extrapolate velocity components projected along any arbitrary direction (except body normal, of course) and the result will be the same. Actually, the general solution of Eqs. (4) and (5) can be expressed as

$$V_1 \cdot \frac{g_{\xi 1}}{|g_{\xi 1}|} = (2V_2 - V_3) \cdot \frac{g_{\xi 1}}{|g_{\xi 1}|} + \frac{R}{\tan\theta} \tag{6}$$

where θ is the angle between A and the body normal. The last term in Eq. (6) is an error contributed by the inconsistency error R and the arbitrary direction of vector A. If A is tangent to the body surface, then the contribution of R in the calculation V_1 is zero resulting [as in Eq. (3)] in the most appropriate velocity component to be extrapolated. In other words, if one wants to enforce a zero normal velocity, the most appropriate procedure, obviously, is to extrapolate the velocity components tangent to the body surface. Now it becomes clear that, in a severely skewed mesh, θ is small and, hence, an extrapolation of the velocity component in the direction of the contravariant base vector $g^{\xi 1}$ will result in a large error. Therefore, it is mainly the extrapolation of the tangential velocity, instead of the contravariant velocity (not the removal of metric variation as claimed in Ref. 2) that decreases the error in the extrapolation for nonorthogonal meshes.

Conclusions

In this Note, we have derived a generalization of extrapolation along an arbitrary direction [Eq. (6)]. Examination of this generalization has clearly pointed out the error associated with the arbitrary direction and has shown that the most appropriate procedure is to extrapolate the velocity components tangent to the body surface. Note that, in a typical calculation, mesh lines are in general clustered and hence are parallel or almost parallel to the body surface. Therefore, the extrapolation used in Ref. 2 will be very close to the discussed extrapolation of velocity components tangent to the body surface, except now the normalization is not necessary.

Caution should be taken that we have confined our discussions only to issues associated with simple linear extrapolation in computational space. The issues of grid line orientation and how to implement an extrapolation, as pointed out in the Introduction, could be more important. All of these indicate room for improvement and also point to the urgency and essentiality of a "good" grid near the body. As a rule of thumb, a grid system should have fine resolution, have minimal variation of mesh spacing near the body, and be nearly straight and normal to the solid body. This is essential for a computation, but is a difficult requirement, especially for a highly irregular geometry.

References

[1]Rizzetta, D. P. and Shang, J. S., "Numerical Simulation of Leading-Edge Vortex Flows," *AIAA Journal*, Vol. 24, Feb. 1986, pp. 237-245.

[2]Pulliam, T. H. and Steger, J. L., "Recent Improvements in Efficiency, Accuracy and Convergence for Implicit Approximate Factorization Algorithms," AIAA Paper 85-360, Jan. 1985.

Stability of Normal Shock Waves in Diffusers

Kazuyasu Matsuo,* Minoru Yaga,† and Hiroaki Mochizuki‡
Kyushu University, Kasuga, Fukuoka, Japan

Received Jan. 20, 1987; revision received March 12, 1987.

*Professor, Graduate School of Engineering Sciences.
†Graduate Student, Graduate School of Engineering Sciences.
‡Research Associate, Graduate School of Engineering Sciences.

Introduction

EXPERIMENTAL evidence shows that a normal shock wave in a supercritical diffuser under a constant overall pressure ratio may display either a stable oscillation about its mean shock position or an unstable oscillation in which shock waves are generated downstream of the throat and move upstream repetitively.[1,2] Culick and Rogers[3] present an analysis of the stability of a shock wave interacting with periodic, low-frequency downstream pressure disturbances. Sajben[4] presents a formula for the trajectory of a stable shock wave in a diffuser. In Refs. 3 and 4, two limiting cases are assumed for the subsonic flow downstream of a shock wave: an isentropic flow and an isobaric flow, the latter being a model for flow separation. In the present Note, the analysis of Culick and Rogers is modified to simulate more realistic diffuser flows by introducing a diffuser efficiency for the subsonic flow downstream of a shock wave.

The governing equation for the interaction between a normal shock and small pressure disturbances p_e' in a diffuser was derived in Eq. (27) of Ref. 3, where the equation was not solved. Integrating this equation with the substitution of $p_e'=\epsilon p_2 \cos\omega t$ $(0<\epsilon\ll 1)$ and with the initial condition of the shock displacement from its initial position $x_s'=0$ at the time $t=0$, we obtain the following equation for the locus of the shock wave:

$$x_s'=\frac{C\epsilon p_2}{1+(\omega\tau)^2}[\sqrt{1+(\omega\tau)^2}\cos(\omega t-\theta)-\exp(-t/\tau)] \tag{1}$$

where

$$\tau=-\frac{1}{a_1 P_s}\left(\frac{1}{s}\frac{dS}{dx}\right)^{-1}\frac{p_1}{p_2}\frac{4\gamma M_1}{\gamma+1} \tag{2}$$

$$C=\frac{1}{p_2 P_s}\left(\frac{1}{S}\frac{dS}{dx}\right)^{-1} \tag{3}$$

$$\theta=\tan^{-1}(\omega\tau) \tag{4}$$

$$P_s=\frac{d\ell n p_1}{d\ell n S}-\frac{d\ell n p_2}{d\ell n S}+\frac{2\gamma}{\gamma+1}\left(\frac{p_1}{p_2}\right)\frac{dM_1^2}{d\ell n S} \tag{5}$$

where a is the velocity of sound, M the flow Mach number, p the static pressure, S the cross-sectional area of the diffuser, ω the angular frequency of the pressure disturbances, and γ the ratio of specific heats, and the subscripts 1 and 2 denote the values at the points immediately upstream and downstream of the shock wave, respectively.

Figure 1 illustrates the streamwise, time-mean pressure distributions. Curve 1 corresponds to an isentropic flow expanding to supersonic Mach numbers, curve 2, denoted by $p_{d,i}(x)$, to an isentropic subsonic flow downstream of the shock wave which is located at $x=x_s$, and curve 3, denoted by $p_d(x)$, a nonisentropic or actual subsonic flow accompanied by separation and friction. Curve 4, denoted by a broken line, represents the locus of the pressure just downstream of the shock wave. For simplicity, assume the following relation:

$$\frac{dp_d}{dx}=\alpha\left(\frac{dp_{d,i}}{dx}\right) \tag{6}$$

where α is a pressure recovery factor; $\alpha=1$ and $\alpha=0$ correspond to an isentropic flow and an isobaric flow downstream of the shock wave, respectively. By applying Eq. (6) to the point 2 immediately downstream of the shock wave, the second term on the right-hand side of Eq. (5), which is not taken into consideration in Ref. 3 because the pressure downstream of the shock wave is assumed to remain constant, can be expressed in terms of α and M_1:

$$\frac{d\ell n p_2}{d\ell n S}=\alpha\frac{\gamma}{\gamma+1}\frac{(\gamma-1)M_1^2+2}{M_1^2-1} \tag{7}$$

Substituting Eq. (7) into Eq. (5), and expressing the first and third terms on the right-hand side of Eq. (5) in terms of M_1, we obtain

$$P_s=-\frac{\gamma\alpha[M_1^2(\gamma-1)+2]}{(\gamma+1)(M_1^2-1)}-\frac{\gamma M_1^2[2M_1^2-(\gamma+3)]}{(M_1^2-1)[2\gamma M_1^2-(\gamma-1)]} \tag{8}$$

If $\alpha=0$, then Eq. (8) reduces to Eq. (47) in Ref. 3. Assuming that α in Eq. (6) remains constant throughout the subsonic flow region downstream of the shock wave and denoting the static pressure at the diffuser exit on curve 2 by $p_{b,i}$ and that on curve 3 by p_b, we obtain

$$p_b-p_2=\alpha(p_{b,i}-p_2) \text{ or } \frac{p_b}{p_2}-1=\alpha\left(\frac{p_{b,i}}{p_2}-1\right) \tag{9}$$

The diffuser efficiency for the subsonic flow downstream of the shock wave, η_{sub}, is defined here by the relation

$$\frac{p_b}{p_2}=\left(1+\frac{\gamma-1}{2}M_2^2\eta_{sub}\right)^{\gamma/(\gamma-1)} \tag{10}$$

If $\eta_{sub}=1$, then p_b in Eq. (10) is equal to $p_{b,i}$. Combining the equation for $p_{b,i}/p_2$ thus obtained with Eqs. (9) and (10) yields an explicit equation for the diffuser efficiency:

$$\eta_{sub}=\frac{2}{(\gamma-1)M_2^2}\left\{\left[\alpha\left(1+\frac{\gamma-1}{2}M_2^2\right)^{\gamma/(\gamma-1)}-(\alpha-1)\right]^{(\gamma-1)/\gamma}-1\right\} \tag{11}$$

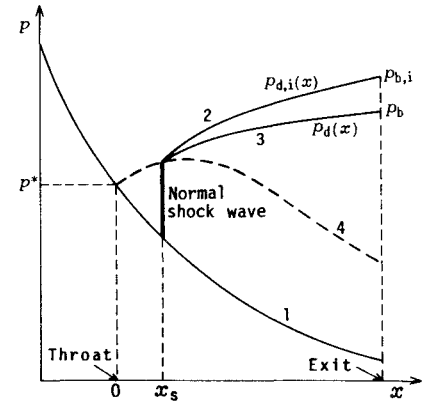

Fig. 1 Static pressure distributions in diffuser.

The trajectory of a shock wave can be calculated by Eq. (1) together with Eqs. (2-4), (8), and (11). Sample calculations were performed for $\gamma=1.4$ and for a two-dimensional diffuser with a circular arc wall contour with a radius of $R=654$ mm and a throat height of $h^*=10$ mm. An example is shown in Fig. 2, where a normal shock at $x_s/\sqrt{Rh^*}=0.2$ ($\sqrt{Rh^*}$ is an appropriate characteristic length for a circular arc diffuser[5]) interacts with a small-amplitude pressure disturbance $p_e'=\epsilon p_2 \cos\omega t$ ($\epsilon=0.1$, $f=\omega/2\pi=500$ Hz) introduced downstream of the shock. The flow Mach number M_1 at $x_s/\sqrt{Rh^*}=0.2$ is calculated from isentropic flow relations, and it is shown that $M_1=1.23$. In Fig. 2, the shock displacement from its initial position x_s' and its nondimensional value $x_s'/\sqrt{Rh^*}$ are shown in the horizontal axis, while

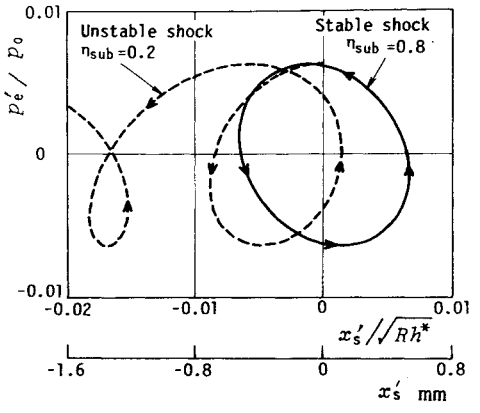

Fig. 2 Trajectories of shock wave in circular arc diffuser: $R=654$ mm, $h^*=10$ mm, $x_s/\sqrt{Rh^*}=0.2$, $M_1=1.23$, $\epsilon=0.01$, $f=500$ Hz.

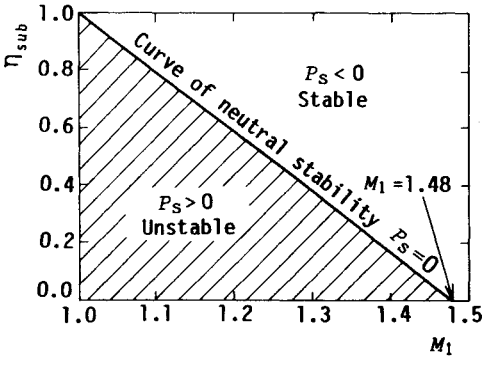

Fig. 3 Curve of neutral stability ($\gamma=1.4$).

the vertical axis represents p_e' divided by the stagnation pressure p_0 upstream of the diffuser; the arrows correspond to increasing time. In the case of $\eta_{sub}=0.8$, the trajectory shows a stable oscillation, whereas in the case of $\eta_{sub}=0.2$, the shock becomes unstable and is propagated upstream. Hence the behavior of the shock wave depends considerably on the diffuser efficiency for the subsonic flow downstream of the shock wave. It is evident from Eq. (1) that for $\tau>0$, the exponential term in Eq. (1) tends to zero and the shock oscillates stably, whereas if $\tau<0$, then x_s' approaches negative infinity, which implies the upstream propagation of the shock wave. For a divergent channel, the signs of τ and P_s are opposite [Eq. (2)]; accordingly, $P_s\leqq 0$ represents a criterion of the stability of the shock wave.

The relation between M_1 and α when $P_s=0$ is obtained from Eq. (8), eliminating α from the relation by the use of Eq. (11), yields the relation between η_{sub} and M_1. A calculated example is shown in Fig. 3. The shaded area where $P_s>0$ represents the unstable region. Figure 3 shows that the lower the Mach number M_1, i.e., the nearer the shock wave approaches the throat in the diffuser, the higher the diffuser efficiency is required for stability. The point of intersection of the curve of neutral stability and the horizontal axis gives $M_1=1.48$, which is the Mach number at which curve 4 in Fig. 1 becomes maximum. If a shock wave appears downstream of this point, the shock wave is always stable, regardless of the diffuser efficiency.

Conclusions

The behavior of a shock wave in a diffuser in response to small-amplitude pressure disturbances has been analyzed. The results suggest as follows:

1) The stability of the shock wave depends not only on the Mach number just upstream of the shock but also on the diffuser efficiency for subsonic flow downstream of the shock wave.

2) The curve of neutral stability that relates the diffuser efficiency η_{sub} to the Mach number M_1 is obtained. For gases with $\gamma=1.4$, the shock wave is always stable regardless of η_{sub} if $M_1>1.48$. For $1<M_1<1.48$, the maximum diffuser efficiency causing instability decreases as M_1 increases.

References

[1]Meier, G.E.A., "Shock Induced Flow Oscillations in a Laval Nozzle," *Symposium Transsonicum II*, edited by K. Oswatitsch and D. Rues, Springer-Verlag, Berlin, 1976, pp. 252–261.

[2]Chen, C. P., Sajben, M., and Kroutil, J. C., "Shock-Wave Oscillations in a Transonic Diffuser Flow," *AIAA Journal*, Vol. 17, Oct. 1979, pp. 1076–1083.

[3]Culick, F.E.C. and Rogers, T., "The Response of Normal Shocks in Diffusers," *AIAA Journal*, Vol. 21, Oct. 1983, pp. 1382–1390.

[4]Sajben, M., "The Response of Normal Shocks in Diffusers," *AIAA Journal*, Vol. 23, March 1985, pp. 477–478.

[5]Wegener, P. P. and Cagliostro, D. J., "Periodic Nozzle Flow with Heat Addition," *Combustion Science and Technology*, Vol. 23, 1973, pp. 269–277.

Unsteady Compressible Laminar Boundary-Layer Formed within a Centered Expansion Wave

T. J. Wang*
Chung-Shan Institute of Science and Technology
Lung-Tan, Taiwan

Introduction

THE purpose of this research is to investigate the effects of viscosity and heat transfer on the unsteady, compressible laminar boundary layer formed within a centered expansion wave traveling into a fluid at rest.[1,2] The temperature is at T_0 initially in the undisturbed high-pressure region. A centered expansion wave is formed at $t=0$ when the diaphram is burst and propagates into the undisturbed region. The qualitative expansion wave boundary layer is shown in Fig. 1. There have been numerous studies of the expansion wave problem.[1,2] It appears that the solutions given via a coordinate expansion of a series expansion method are restricted to the early stage of flow development. These results are less accurate for stations further downstream or later in time since the accuracy depends on the scale of the step size.

The present Note provides accurate and extensive solutions for a centered expansion wave advancing into quiescent fluid using the method of semisimilar solutions. The skin-friction distribution and heat-transfer distribution on the wall as determined by the present analysis are proven accurate by comparison with previous studies. The present study also presents results that are applicable at larger distances or at later times in the development of a centered expansion wave.

Received Dec. 3, 1986; revision received March 9, 1987.

*Research Assistant. Member AIAA.